

Dynamics of Evanescently-Coupled Laser Pairs With Unequal Pumping: Analysis Using a Three-Variable Reduction of the Coupled Rate Equations

Mike Adams , Rihab Al Seyab , Ian Henning , Hadi Susanto , and Martin Vaughan 

Abstract—The five coupled rate equations used to describe laterally-coupled pairs of lasers with weak coupling and unequal pumping are reduced to a new system of three equations. This enables approximate closed-form steady-state solutions and explicit expressions for the boundaries between regions of stable and unstable dynamics to be found. The results of applying these approximations to specific cases of coupled laser pairs are shown to be in good agreement with results obtained from numerical solutions of the original set of five equations as well as earlier results from the literature. In addition the approximations based on the reduced set of equations allow a systematic investigation of the effects of material, device and operating conditions on trends and novel features in the dynamics of laterally-coupled laser pairs. The algebraic results give insight into trends with parameters without the need for extensive numerical computation and should therefore be of use in modelling two-element VCSEL arrays for numerous potential applications.

Index Terms—Laser dynamics semiconductor laser arrays, stability analysis.

I. INTRODUCTION

THE study of small arrays of coupled semiconductor lasers, especially those with independent control of pumping for each element [1]–[4], is an area which is receiving increasing interest and attention. For the case of VCSEL arrays this has been driven by attractive properties including phase front engineering and beam-steering [5],[6], extended bandwidth [7],[8] and enhanced digital modulation [9],[4], with one exemplar application being the prospect of tunable ultrafast photonic oscillators [10],[11]. At the fundamental level, such arrays have been

Manuscript received February 8, 2021; revised April 22, 2021; accepted April 23, 2021. Date of publication April 28, 2021; date of current version July 16, 2021. This work was supported by the Engineering and Physical Sciences Research Council (EPSRC) under Grant EP/M024237/1. (Corresponding author: Mike Adams.)

Mike Adams, Ian Henning, and Martin Vaughan are with the School of Computer Science and Electronic Engineering, University of Essex, Colchester CO4 3SQ, U.K. (e-mail: adammm@essex.ac.uk; idhenn@essex.ac.uk; martinpaul.vaughan@physics.org).

Rihab Al Seyab is with the School of Computing and Engineering, University of Gloucestershire, Cheltenham GL50 2RH, U.K. (e-mail: ralseyab@glos.ac.uk).

Hadi Susanto is with the Department of Mathematics, Khalifa University of Science and Technology, Abu Dhabi 127788, UAE, and also with the Department of Mathematical Sciences, University of Essex, Colchester CO4 3SQ, U.K. (e-mail: hsusanto@essex.ac.uk).

Color versions of one or more figures in this article are available at <https://doi.org/10.1109/JSTQE.2021.3076083>.

Digital Object Identifier 10.1109/JSTQE.2021.3076083

shown to exhibit non-Hermiticity [12],[13], exceptional points [13]–[15] and parity-time symmetry breaking [1]. Theoretical understanding and modelling of these effects has been largely based on coupled rate equations [1],[2],[10]–[12],[14]–[16]. These apply in the general case of unequal pumping and have also been extended to include asymmetry in coupling coefficient and photon and carrier lifetimes [17]. Since there is a dearth of analytical solutions, numerical methods have largely been necessary to explore the importance of key physical design and material parameters. While numerical methods have proved effective in many cases, analytic solutions can often provide more accessible routes and clearer insights towards understanding the system. For the particular case of weakly-coupled 2-element arrays with equal pumping, approximate steady-state solutions as well as analytic expressions for the boundaries of regions of stability have been presented [16]. Thus the objective of the present contribution is to extend that work so as to provide approximations for these quantities in the case of unequal pumping in weakly-coupled laser pairs with symmetric real coupling.

This paper is organised as follows. Section II presents the main theoretical results in terms of a reduction of the five coupled rate equations to a new system of three equations, as well as the approximate algebraic solutions of these equations and three stability conditions for their dynamics. Details of the derivations of these results are given in Appendices A and B. Section III presents first some tests of these results against published work and then proceeds to give some examples of the use of the approximate stability boundaries for a specific example. The accuracy of these approximations is demonstrated by comparison with stability maps calculated using the method of Langrangian descriptors [18] as well as by numerical integration of the rate equations combined with a bifurcation method [19]. It is shown that the approximate solutions permit novel features of the dynamic maps to be identified and their dependence on coupling coefficient and pumping asymmetry to be explored in a systematic manner. These features are summarised in the concluding section IV.

II. THEORY

We begin with the rate equations for a pair of coupled lasers whose coupling rate η is real [16]:

$$\frac{dY_A}{dt} = \frac{1}{2\tau_p} (M_A - 1) Y_A - \eta Y_B \sin \phi \quad (1)$$

$$\frac{dY_B}{dt} = \frac{1}{2\tau_p} (M_B - 1) Y_B + \eta Y_A \sin \phi \quad (2)$$

$$\frac{d\phi}{dt} = \frac{\alpha_H}{2\tau_p} (M_A - M_B) - \Delta\Omega + \eta \left(\frac{Y_A}{Y_B} - \frac{Y_B}{Y_A} \right) \cos \phi \quad (3)$$

$$\frac{dM_{A,B}}{dt} = \frac{1}{\tau_N} [Q_{A,B} - M_{A,B} (1 + Y_{A,B}^2)] \quad (4)$$

where Y_A, Y_B are the normalised fields and M_A, M_B are the normalised carrier densities in lasers A, B, respectively, ϕ is the phase difference between the fields in B and A, $\Delta\Omega$ is the detuning between the cavity resonances of lasers B and A, τ_N is the carrier lifetime, τ_p is the photon lifetime, α_H is the linewidth enhancement factor and Q_A, Q_B are the normalised pumping rates. We assume weak coupling, hence $\eta\tau_p \ll 1$.

Now, following earlier approaches for VCSELs [20],[21], ring lasers [22] and spin-VCSELs [23], assume that $\tau_p \ll \tau_N$ and $M_{A,B} - 1 \ll 1$. Hence define $M_A = 1 + m_A, M_B = 1 + m_B$ with $m_A, m_B \ll 1$. It follows that (1) – (4) can be reduced to three rate equations and one conservation relation, as follows:

$$\frac{dm}{dt} = \frac{1}{\tau_N} \left[(Q_A + Q_B - 2) \left(q + \sin \psi - \frac{m \cos^2 \psi}{2} \right) - m \right] \quad (5)$$

$$\frac{d\phi}{dt} = \frac{\alpha_H m}{2\tau_p} - \Delta\Omega - 2\eta \cos \phi \tan \psi \quad (6)$$

$$\frac{d\psi}{dt} = -m \frac{\cos \psi}{2\tau_p} + 2\eta \sin \phi \quad (7)$$

$$Q_A + Q_B - 2 = Y_A^2 + Y_B^2 \quad (8)$$

The new variables are defined by $q = (Q_A - Q_B) / (Q_A + Q_B - 2)$, $m = m_A - m_B$ and $Y_B/Y_A = \tan(\psi/2 + \pi/4)$, and the details of the derivation of these equations are given in Appendix A. Equation (8) is an energy conservation law that holds on the timescale of the carrier recombination time, whilst shorter timescale dynamics are included in (5)-(7). The steady state solutions of (5) – (7) can be found explicitly by using the approximation $\sin \psi_s \cong -q$ which is consistent with $\eta\tau_p \ll 1, m_s \ll 1$, where the subscript ‘s’ denotes the steady-state value. The results can then be written as

$$m_{As} \cong 2\eta\tau_p \sqrt{\frac{Q_B - 1}{Q_A - 1}} \sin \phi_s \quad m_{Bs} \cong -2\eta\tau_p \sqrt{\frac{Q_A - 1}{Q_B - 1}} \sin \phi_s \quad (9)$$

$$Y_{As} \cong \sqrt{(Q_A - 1)} \quad Y_{Bs} \cong \sqrt{(Q_B - 1)} \quad (10)$$

$$\Delta\Omega = \frac{2\eta}{\sqrt{1 - q^2}} (\alpha_H \sin \phi_s + q \cos \phi_s) \quad (11)$$

In the limit of equal pumping $Q_A = Q_B, q = 0$, (9) and (11) reduce to the forms in (25), (26) and (29) of [16], whilst (10) reduces to the forms of (27) and (28) of [16] but without the terms of order $\eta\tau_p$ which appear in the latter. Since we assume

$\eta\tau_p \ll 1$, this omission should only result in a very small error in the accuracy of (10).

We distinguish between the situations of ‘tilted in-phase’ and ‘tilted out-of-phase’ solutions of (5) – (7), following the nomenclature introduced by Gao et al [12]. It follows from (11) that the steady-state phase values, denoted ϕ_{s+} and ϕ_{s-} , respectively, for these solutions are given by tilted in-phase:

$$\phi_{s+} = \arcsin \left(\frac{\Delta\Omega}{2\eta} \sqrt{\frac{1 - q^2}{\alpha_H^2 + q^2}} \right) - \arctan \left(\frac{q}{\alpha_H} \right) \quad (12a)$$

tilted out-of-phase:

$$\phi_{s-} = \pi - \arcsin \left(\frac{\Delta\Omega}{2\eta} \sqrt{\frac{1 - q^2}{\alpha_H^2 + q^2}} \right) - \arctan \left(\frac{q}{\alpha_H} \right) \quad (12b)$$

For equal pumping these reduce to the forms $\phi_{s+} = \arcsin(\Delta\Omega/2\alpha_H\eta)$, $\phi_{s-} = \pi - \phi_{s+}$ given in [12].

By performing a small-signal analysis of (5) – (7) (see Appendix B), approximate expressions for the stability boundaries of the system can be found as:

$$[(Q_A + Q_B)(1 - q^2) + 2q^2] \sqrt{(1 - q^2)} + 8\eta\tau_N q \sin \phi_s > 0 \quad (13)$$

$$|\Delta\Omega| < 2\eta \sqrt{\frac{\alpha_H^2 + q^2}{1 - q^2}} \quad (14)$$

$$[(Q_A + Q_B)(1 - q^2) + 2q^2] \sqrt{1 - q^2} + 4\eta\tau_N (\alpha_H \cos \phi_s + q \sin \phi_s) > 0 \quad (15)$$

Equation (15), in combination with (11), corresponds to the Hopf bifurcation. Equation (14) describes the saddle-node (SN) bifurcation. For this upper limit of detuning, (12a) and (12b) show that the phase values for the in-phase and out-of-phase solutions are equal:

$$|\Delta\Omega| = 2\eta \sqrt{\frac{\alpha_H^2 + q^2}{1 - q^2}} \quad \phi_{s+} = \phi_{s-} = \frac{\pi}{2} - \arctan \left(\frac{q}{\alpha_H} \right) \quad (16)$$

In the limit of equal pumping the results of (14) and (15) can be reduced to the forms of (30) and (31) of [16] for real coupling rate, i.e.,

$$q = 0 : \quad 2\alpha_H\eta \sqrt{1 - \left[\frac{Q}{2\tau_N\alpha_H\eta} \right]^2} < |\Delta\Omega| < 2\alpha_H\eta \quad (17)$$

where $Q = Q_A \equiv Q_B$.

Equations (5) – (15) are the main results of this paper. In the following we test them against results in the literature and give some numerical examples of their use. The accuracy of results for these examples is verified using different numerical methods of solution.

III. RESULTS

A. Comparison With Results From the Literature

The accuracy of the approximations used in deriving (9) – (15) can be tested by comparing some results with those in the literature. First, for the steady-state solutions we compare with the results of Erneux and Lenstra [24] in their special case of zero time delay of mutually delay-coupled quantum cascade lasers. These authors use similar assumptions of weak coupling to reduce the six rate equations for that system to two coupled equations for the phase of the electric fields; for the case of zero time delay these can be combined into a single equation. It is straightforward to show that our (10) and (11) can be combined in the form

$$\Delta\Omega = -\eta\sqrt{1 - \alpha_H^2} \left[\frac{Y_A}{Y_B} \sin(\theta_o - \phi_s) - \frac{Y_B}{Y_A} \sin(\theta_o + \phi_s) \right] \quad (18)$$

where $\theta_o = \tan^{-1}(\alpha_H) - \pi/2$. This result matches the steady-state solution of the corresponding phase equation (12) of [24], allowing for the differences in notation.

Contours of constant phase ϕ_{s+} , ϕ_{s-} and field ratio Y_B/Y_A in the plane of Q_B versus $\Delta\Omega$ for fixed Q_A , calculated from a numerical root searching technique, have been presented by Gao *et al* in [12]. The steady-state results (10) and (12) can be used to allow comparison with these; similarly the boundaries of stable operation can be found from (14) and (15). Using the parameter values corresponding to the weakly-coupled ‘‘array 1’’ ($\eta\tau_p = 0.002$) of [12] with $Q_A = 3.2$, the results of applying our equations to find tilted in-phase and out-of-phase solutions show good agreement for contours of constant phase. Encouraging agreement is also found for the limits of stability using the SN bifurcation approximation from (14). In addition we calculated the Hopf bifurcation using (15) and (11). For this we needed the value of τ_N which is not given in [12]; since in other publications, e.g., [8],[17],[25], these authors use $\tau_N = 2$ ns, that value was assumed here. Our results indicate that only the out-of-phase case shows stability and moreover the range of stable solutions, as bounded these bifurcations, is very limited for this array. Stability is restricted to two narrow regions: one at negative detuning for $Q_B > Q_A$ with phase close to $3\pi/2$ and the other at positive detuning for $Q_B < Q_A$ with phase close to $\pi/2$.

Contours of constant phase as well as boundaries of stable operation in the plane of normalised detuning versus normalised pumping difference are presented by Kominis *et al* in [14] for very weak coupling ($\eta\tau_p = 0.000315$). Hence for a further test of our approximate results (13) – (15) we used the same parameters as [14]. The plot that appears as Figure 9(b) of [14], calculated by utilising a numerical continuation algorithm, applies to the range ($0 \leq q \leq 1, 0 \leq -\Delta\Omega\tau_p/0.05 \leq 0.15$) in the plane of normalised detuning $-\Delta\Omega\tau_p/0.05$ ($\equiv \Delta'$ [14]) versus q ($\equiv 2 \times \Delta P'$ [14]). For this range our results for the tilted out-of-phase solutions of this system are in very good agreement with those presented in [14]. Note that comparison of our (3) with (6) of [14] indicates that the minus sign in the detuning is needed for comparison of results.

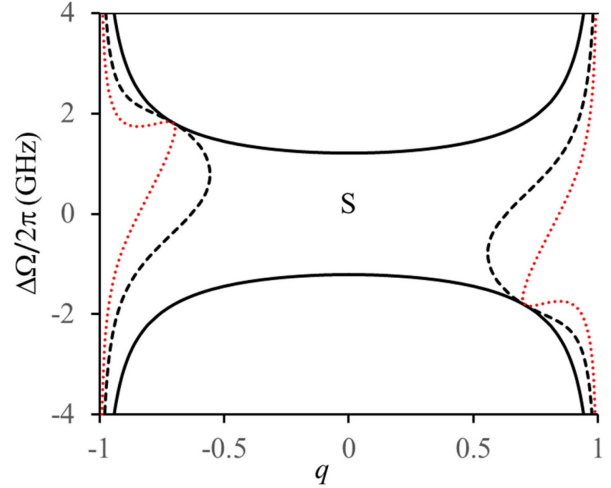


Fig. 1. Stability boundaries from (13) – (15) in the plane of normalised detuning versus q for parameters $\alpha_H = 2$, $\tau_N = 1$ ns, $\tau_p = 1.53$ ps, $\eta = 1.908$ ns $^{-1}$ and $Q_A + Q_B = 26.8$. ‘S’ denotes the region of stable operation.

Comparison of the results discussed above using parameters from [12] and [14], leaving aside the difference of axes related to pumping rate, reveals a significant difference between the topology of the regions of stability for each case. As mentioned above, in the case of parameters from [12] there are separate distinct regions of stability for positive q ($Q_A > Q_B$) and negative q ($Q_A < Q_B$), each bounded by a pair of SN and Hopf bifurcations. In contrast, we find for parameters from [14] there is a single stable region that includes both negative and positive q and is bounded by two SN and two Hopf bifurcations. This difference can be traced to the difference in relative sets of parameters and can be quantified in terms of a critical value η_c of the coupling rate given by the condition that the square root in (17) vanishes for the case of equal pumping, i.e., $\eta_c = Q/(2\tau_N\alpha_H)$ where $Q = Q_A = Q_B$. For values of coupling rate that are greater than or equal to η_c the argument of the square root in (17) is greater than zero and the regions of stability are similar to those for parameters of [12] where $\eta = 1$ and $\eta_c = 0.2$ with our assumption of $\tau_N = 2$ ns. For values of coupling rate that are less than η_c the regions of stability are similar to those for parameters of [14] where $\eta\tau_p = 0.000315$ and $\eta_c\tau_p = 0.0005$.

B. Numerical Results for a Specific Example

Consider the case of real index slab wave-guiding [16] with $\alpha_H = 2$, $\tau_N = 1$ ns, $\tau_p = 1.53$ ps and $\eta = 83.6 \exp(-2.52 d/a)$ ns $^{-1}$ where $2d$ is the edge-to-edge separation of the laser waveguides and $2a$ is the width of each. The normalised pumping rate $Q_{A,B}$ in each laser is related to the physical pumping rate $P_{A,B}$ by $Q_j = 11.4(P_j/P_{jth} - 1) + P_j/P_{jth}$ where the subscript ‘th’ denotes the value at lasing threshold. We will consider only the tilted out-of-phase solutions since these are the only ones allowed for these parameters at $q = 0$ [16]. First we consider the case of laser separation given by $d = 1.5a$, which yields $\eta = 1.908$ ns $^{-1}$ ($\eta\tau_p = 0.00292$), with $Q_A + Q_B = 26.8$ which corresponds to both lasers at twice threshold when $q = 0$. Fig. 1 shows a stability map in the plane of linear frequency detuning $\Delta\Omega/2\pi$

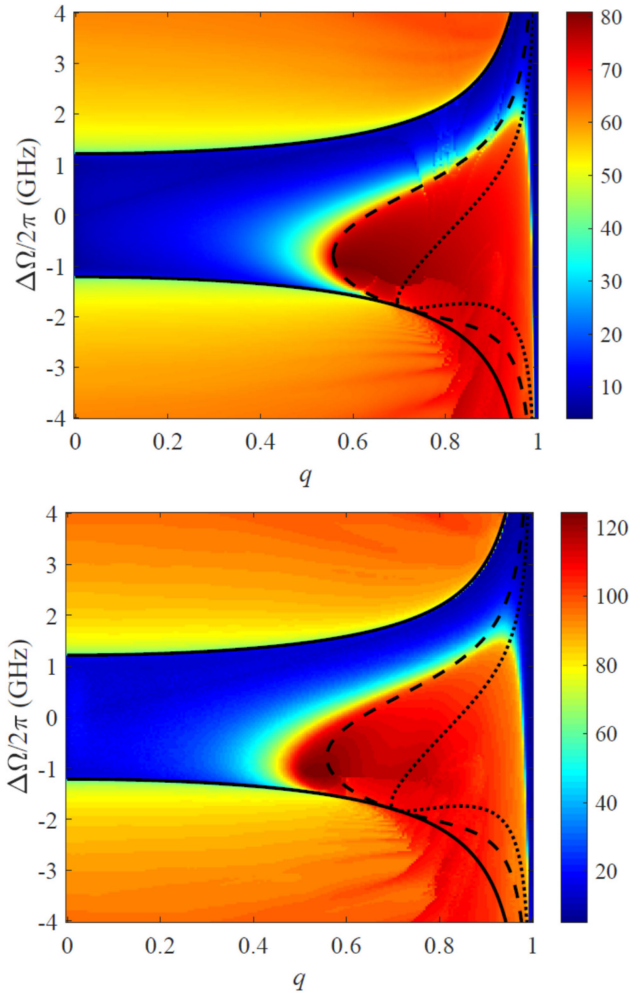


Fig. 2. Stability maps in the plane of normalised detuning versus positive q for the same parameters as in Fig. 1, calculated using the method of Lagrangian descriptors: (top) for the 3 reduced equations (5) – (7), and (bottom) for the full set of equations (1) – (4). Blue colour denotes the region of stable operation. The stability boundaries from (13) – (15) are also shown.

versus q , where the dotted red, solid black and broken black lines correspond to the stability boundaries defined by (13), (14) and (15), respectively. The region of stable operation is bounded by two SN and two Hopf bifurcations, as defined by (14) and (15). This is because the critical value of coupling η_c for these parameters is 3.35 ns^{-1} which is greater than the value of 1.908 ns^{-1} used to calculate Fig. 1. There are two points in Fig. 1 where the 3 boundary lines touch tangentially; these SN-Hopf points are at $(0.7072, -1.822 \text{ GHz})$ and $(-0.7072, 1.822 \text{ GHz})$. It is easy to show that these points are given by $\tan\phi_s = \alpha_H/q$.

In order to verify the accuracy of our approximations, stability maps have been calculated using the method of Lagrangian descriptors (LDs) [18]. These are shown in Fig. 2 for the reduced equations (5) – (7), and the full set of equations (1) – (4). Only the positive q half-plane is shown in each case. The colour shading indicates the contours of the Lagrangian descriptor for the system. Bifurcations are indicated by abrupt changes in these contours. Fig. 2(top) thus tests the accuracy of the approximation $\sin\psi_s \cong -q$ which is used in deriving the stability boundaries

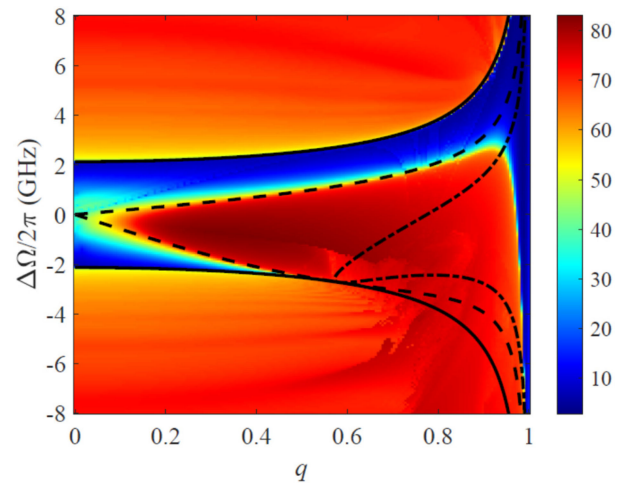


Fig. 3. Stability map with boundaries from (13) – (15) in the plane of normalised detuning versus q with $\eta = 3.35 \text{ ns}^{-1}$ and other parameters as for Fig. 1. Blue colour denotes the regions of stable operation.

(13) – (15) (see Appendix B). These boundaries are seen to be in good agreement with the LD result in defining the region of stable operation (denoted by blue colour). Fig. 2(bottom) verifies the accuracy of the reduced set of equations (5) – (7) since there is good agreement with Fig. 2(top), the only small difference occurring in the position of the Hopf bifurcation at its region of lowest q (around 0.5).

For the next example, we take the coupling rate to be the critical value of 3.35 ns^{-1} ($\eta\tau_p = 0.00513$), keeping the other parameter values the same as those for Fig. 1. This value of η corresponds to a spacing of $d = 1.2766a$ in the model of coupled slab waveguides [16]. Fig. 3 shows the boundaries defined by (13) – (15) superimposed on an LD stability map using (4) – (7). Only the positive q half-plane is shown since the negative half-plane can be found by simply reversing the signs of the axes. There are two regions of stable behaviour (in blue) each of which is enclosed by saddle-node and Hopf bifurcations, and the latter boundaries intersect at $q = 0$. In this case the points of contact of lines defined by (13) – (15) are at $(0.5818, -2.7308 \text{ GHz})$ and $(-0.5818, 2.7308 \text{ GHz})$. There is a good level of agreement between the approximate boundaries and those found from the LD method with an error increasing at values of q close to 1.

To complete this set of results we consider a higher rate of coupling given by $\eta = 6.726 \text{ ns}^{-1}$ ($\eta\tau_p = 0.0103$), corresponding to a spacing of $d = a$, i.e., the edge-to-edge spacing is equal to the full width of each waveguide. Fig. 4 shows two regions of stable behaviour each of which is enclosed by SN and Hopf bifurcations which meet at the points $(0.3977, -4.7585 \text{ GHz})$ and $(-0.3977, 4.7585 \text{ GHz})$. Again the agreement between approximation and LD boundaries is good except at higher values of q .

Another way to present these results is in terms of detuning versus normalised laser spacing d/a for various values of the normalised pumping difference q . Fig. 5 shows plots of this type for q values of 0.4 and 0.8, using the same parameters as those used previously. In Fig. 5(top) the condition for equality of the boundaries occurs for $d/a = 1$ at $q = 0.3977$ as mentioned in the

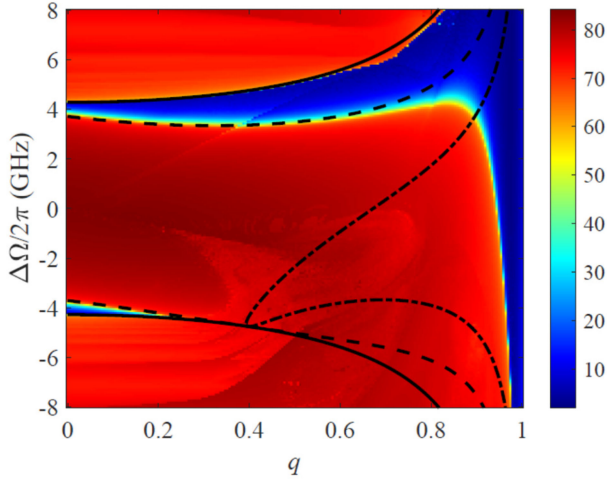


Fig. 4. Stability map with boundaries from (13) – (15) in the plane of normalised detuning versus q with $\eta = 6.726 \text{ ns}^{-1}$ and other parameters as for Fig. 1. Blue colour denotes the regions of stable operation.

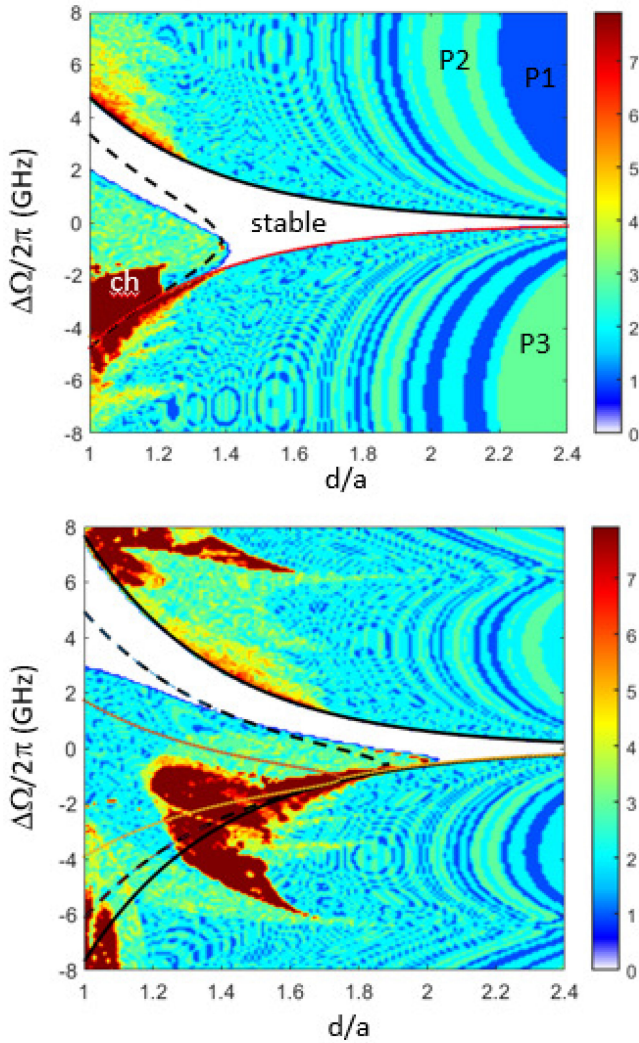


Fig. 5. Stability maps and boundaries from equations (13) – (15) in the plane of normalised detuning versus normalised spacing d/a for $q = 0.4$ (top) and 0.8 (bottom) and other parameters as for Fig. 1. The scale on the colour bar shows the numbers of extrema in the time series.

discussion of Fig. 4; hence for the value of $q = 0.4$ used here the curve for (13) is barely observable. For $q = 0.8$ in Fig. 5(bottom) the change of all boundaries is clearly seen, as expected from the discussion of Figs. 1 – 4.

In order to test the accuracy of the approximations used to produce Fig. 5, a numerical (Runge-Kutta) solution of the rate equations (1) – (4) was used. From the extrema of the time series of $Y_A^2 + Y_B^2 + 2Y_A Y_B \cos \phi$ at each value of d/a and detuning, one-parameter bifurcation diagrams are used to construct the stability maps in Fig. 5. Examples of one-parameter bifurcation diagrams are given in Figs 5 and 9 of [16] and details of how these are used to construct stability maps are given in [19]. White colour is used to denote the regions of stability; other colours denoting regions of period 1, 2 and 3 oscillation and chaos are marked in Fig. 5(top). It is clear that there is a very good level of agreement for the larger values of d/a , whilst at smaller values the approximate results tend to underestimate the frequency range of the stable region. The SN bifurcations agree well and the underestimate is associated with error in the Hopf curves at higher coupling rates. This is thought to be associated with the small error (of order $\eta\tau_p$) which was noted in the discussion of (10) in section II and implies an error of the same order in the approximation $\sin \psi_s \cong -q$. Thus, based on this evidence and that from the comparisons of results in Fig. 4, we estimate that the approximation of (15) for the Hopf bifurcation is very accurate provided $\eta\tau_p$ is less than about 0.005. No such limit appears to apply to the approximation of (14) for the SN bifurcation which retains its accuracy over the entire range tested here.

IV. CONCLUSION

In this paper we report on how the five coupled rate equations which describe laterally coupled laser pairs with weak real coupling ($\eta\tau_p \ll 1$) can be reduced to a system of three equations. The variables in these equations are the phase difference between the fields in the two lasers, the ratio of the field amplitudes (expressed as an angle) and the difference in normalised excess carrier densities in the two lasers. The underlying physical parameters are the coupling rate η , the linewidth enhancement factor α_H , the carrier lifetime τ_N , the photon lifetime τ_p , the detuning $\Delta\Omega$ between the cavity resonances of the lasers and the normalised pumping rates expressed in terms of their sum ($Q_A + Q_B$) and relative difference $q = (Q_A - Q_B)/(Q_A + Q_B - 2)$. The approximate steady-state solutions of this reduced set of equations have been tested against published results which were found using numerical methods. Additionally, the use of a small-signal analysis has revealed closed-form expressions which predict the boundaries of stable operation. These have also been compared against published results and our own numerical solutions for the case of weakly-coupled laser pairs, and good agreement between the numerical methods and those from the approximations are found. Finally, in the limit of equal pumping the algebraic approximations are shown to reduce to those already known from earlier work [16],[26].

The new closed-form expressions allow a systematic investigation of the dependence of the dynamics on parameters such as pumping rates, coupling rate and linewidth factor. Results

have been presented for a specific example showing the effect of varying η and q whilst keeping $(Q_A + Q_B)$ fixed. These results show novel effects in terms of the asymmetric behaviour of the stability boundaries and how this develops as the parameter values are changed. In all cases analysed it is found that pairs of saddle-node and Hopf bifurcations touch tangentially at points whose co-ordinates can be found algebraically. In addition the new expressions offer a route for future exploration of the various forms of nonlinear dynamics that exist in a system of coupled laser pairs in terms of physical designs and materials parameters, and via external control using differential pumping. Such results should be useful in modelling 2-element VCSEL arrays for applications such as beam steering, enhanced modulation response, etc., since trends with various parameters can easily be tracked without the need for extensive numerical simulation.

The approach used here follows a method applied previously to VCSELs [20],[21],[23] and ring lasers [22] in that a reduction in the number of rate equations is achieved by assuming a power conservation law and a new variable that is related to the ratio of the field amplitudes. This approach would also be applicable to coupled nanowire lasers which have been predicted to have potential for ultra-high frequency modulation [27]. Whilst the present contribution has been limited to the case of real coupling rates, it is straightforward to extend this to take account also of the phase of the coupling in order to give a more general description of the effects of gain-guiding and index antiguiding [16]. Further generalisation to deal with larger arrays of weakly-coupled lasers, including two-dimensional arrays of VCSELs, is also possible but in all cases it is only possible to reduce the number of rate equations by two.

APPENDIX A

DERIVATION OF THE REDUCED SET OF COUPLED RATE EQUATIONS

Defining $M_A = 1 + m_A$, $M_B = 1 + m_B$ with $m_A, m_B \ll 1$, adding and subtracting the two versions of (4) yields

$$\frac{d(m_A + m_B)}{dt} = \frac{1}{\tau_N} [Q_A + Q_B - 2 - (Y_A^2 + Y_B^2) - (m_A Y_A^2 + m_B Y_B^2) - (m_A + m_B)] \quad (\text{A1})$$

$$\frac{d(m_A - m_B)}{dt} = \frac{1}{\tau_N} [Q_A - Q_B - (Y_A^2 - Y_B^2) - (m_A Y_A^2 - m_B Y_B^2) - (m_A - m_B)] \quad (\text{A2})$$

For the situation of $\eta\tau_p \ll 1$ we will assume that (A1) can be replaced by a conservation law that holds for dynamic time scales longer than the relaxation oscillation period:

$$Q_A + Q_B = 2 + Y_A^2 + Y_B^2 \quad (\text{A3})$$

We have thus assumed that the time derivative in (A1) is zero and that the final two terms on the RHS can be neglected. We show below in (A5) that the penultimate term is zero.

From (A3) it follows that

$$\frac{d[Y_A^2 + Y_B^2]}{dt} = 0 \quad (\text{A4})$$

Using (1) and (2) this result leads to

$$m_A Y_A^2 + m_B Y_B^2 = 0 \quad (\text{A5})$$

Following the example of [22], we define a new variable ψ by using again the conservation law (A3):

$$Y_A = \sqrt{\Pi} \cos\left(\frac{\psi + \pi/2}{2}\right) \quad Y_B = \sqrt{\Pi} \sin\left(\frac{\psi + \pi/2}{2}\right) \quad (\text{A6})$$

where $\Pi = Q_A + Q_B - 2$. It follows that (A5) can be written as

$$m_A Y_A^2 + m_B Y_B^2 = \Pi \frac{m_A (1 - \sin \psi) + m_B (1 + \sin \psi)}{2} = 0 \quad (\text{A7})$$

Hence, neglecting the trivial (threshold) case $Q_A + Q_B = 2$, it follows that in general

$$m_A + m_B = (m_A - m_B) \sin \psi \quad (\text{A8})$$

It follows that

$$m_A Y_A^2 - m_B Y_B^2 = \frac{\Pi (m_A - m_B) \cos^2 \psi}{2} \quad (\text{A9})$$

Using this result and the definitions (A6), (A2) becomes

$$\begin{aligned} & \frac{d(m_A - m_B)}{dt} \\ &= \frac{1}{\tau_N} \left\{ Q_A - Q_B + \Pi \left[\sin \psi - \frac{(m_A - m_B) \cos^2 \psi}{2} \right] - (m_A - m_B) \right\} \end{aligned} \quad (\text{A10})$$

Also, (3) becomes

$$\frac{d\phi}{dt} = \frac{\alpha_H}{2\tau_p} (m_A - m_B) - \Delta\Omega - 2\eta \cos \phi \tan \psi \quad (\text{A11})$$

From the definitions (A6), we have

$$\begin{aligned} \frac{dY_A}{dt} &= -\frac{Y_A}{2} \tan\left(\frac{\psi + \pi/2}{2}\right) \frac{d\psi}{dt} \\ \frac{dY_B}{dt} &= \frac{Y_B}{2} \cot\left(\frac{\psi + \pi/2}{2}\right) \frac{d\psi}{dt} \end{aligned} \quad (\text{A12})$$

Hence (1) and (2) can be transformed to

$$\frac{d\psi}{dt} = -\frac{m_A}{\tau_p} \cot\left(\frac{\psi + \pi/2}{2}\right) + 2\eta \sin \phi \quad (\text{A13})$$

$$\frac{d\psi}{dt} = \frac{m_B}{\tau_p} \tan\left(\frac{\psi + \pi/2}{2}\right) + 2\eta \sin \phi \quad (\text{A14})$$

Multiplying (A13) by $\tan[(\psi + \pi/2)/2]$ and (A14) by $\cot[(\psi + \pi/2)/2]$, and adding gives

$$\frac{d\psi}{dt} = -(m_A - m_B) \frac{\cos \psi}{2\tau_p} + 2\eta \sin \phi \quad (\text{A15})$$

Defining new variables $m = m_A - m_B$ and $q = (Q_A - Q_B)/\Pi$, (A10), (A11) and (A15) can be written as

$$\frac{dm}{dt} = \frac{1}{\tau_N} \left[\Pi \left(q + \sin \psi - \frac{m \cos^2 \psi}{2} \right) - m \right] \quad (\text{A16})$$

$$\frac{d\phi}{dt} = \frac{\alpha_H m}{2\tau_p} - \Delta\Omega - 2\eta \cos\phi \tan\psi \quad (\text{A17})$$

$$\frac{d\psi}{dt} = -m \frac{\cos\psi}{2\tau_p} + 2\eta \sin\phi \quad (\text{A18})$$

These are the reduced set of equations given as (5) – (7) in the main text. The steady state versions are

$$2\Pi(q + \sin\psi_s) = \Pi m_s \cos^2\psi_s + 2m_s \quad (\text{A19})$$

$$\Delta\Omega = \frac{2\eta}{\cos\psi_s} (\alpha_H \sin\phi_s - \cos\phi_s \sin\psi_s) \quad (\text{A20})$$

$$m_s = 4\eta\tau_p \frac{\sin\phi_s}{\cos\psi_s} \quad (\text{A21})$$

where the subscript ‘s’ denotes the steady-state value. Since we assume that $\eta\tau_p \ll 1$, $m_s \ll 1$, it follows that a good approximation for the solution of (A19) is

$$\sin\psi_s \cong -q \quad (\text{A22})$$

Using this approximation in (A21) and (A8) it follows that

$$m_{As} \cong 2\eta\tau_p \sqrt{\frac{1-q}{1+q}} \sin\phi_s \quad m_{Bs} \cong -2\eta\tau_p \sqrt{\frac{1+q}{1-q}} \sin\phi_s \quad (\text{A23})$$

In the limit of equal pumping $q = 0$, these results reduce to the expressions given in [16] in the case of real coupling. In the limits of q tending to 1 or -1, which correspond, respectively, to $Q_B = 1$ or $Q_A = 1$, i.e., one or other laser at threshold, the result in (A23) for the laser above threshold suggests that the quantity m_j tends to infinity. However, this is also the case for the steady-state solutions of (1) and (2) since at threshold the field amplitude is zero.

APPENDIX B

STABILITY ANALYSIS OF THE REDUCED SET OF EQUATIONS

The perturbed solutions of (A16) – (A18) are $m = m_s + \Delta m e^{\lambda t}$, $\phi = \phi_s + \Delta\phi e^{\lambda t}$ and $\psi = \psi_s + \Delta\psi e^{\lambda t}$ where $\Delta m \ll m_s$, $\Delta\phi \ll \phi_s$ and $\Delta\psi \ll \psi_s$. It follows that, to first order in small quantities, the resulting equations can be combined into a cubic equation of the form

$$\lambda^3 + A_1\lambda^2 + A_2\lambda + A_3 = 0 \quad (\text{B1})$$

where the coefficients A_i are given by

$$A_1 = \frac{\Pi \cos^2\psi_s + 2}{2\tau_N} - 4\eta \sin\phi_s \tan\psi_s \quad (\text{B2})$$

$$A_2 = -\frac{(\Pi \cos^2\psi_s + 2)}{\tau_N} 2\eta \sin\phi_s \tan\psi_s + 4\eta^2 \left[(\sin\phi_s \tan\psi_s)^2 + \left(\frac{\cos\phi_s}{\cos\psi_s} \right)^2 \right] + \Pi (\cos\psi_s + 4\eta\tau_p \sin\psi_s \sin\phi_s) \frac{\cos\psi_s}{2\tau_p\tau_N} \quad (\text{B3})$$

$$A_3 = \frac{(\Pi \cos^2\psi_s + 2)}{\tau_N} 2\eta^2 \left[(\sin\phi_s \tan\psi_s)^2 + \left(\frac{\cos\phi_s}{\cos\psi_s} \right)^2 \right] - \frac{\Pi}{\tau_p\tau_N} \eta (\cos\psi_s + 4\eta\tau_p \sin\psi_s \sin\phi_s) (\alpha_H \cos\phi_s + \sin\phi_s \sin\psi_s) \quad (\text{B4})$$

For the case of equal pumping, $q = 0$, $\Pi = 2(Q - 1)$, $\sin\psi_s = 0$, (B2) – (B4) are identical to (B17) – (B19) in [16] (with $\eta_i = 0$).

The conditions for stable steady-state solutions of (B7) are

$$A_1 > 0, \quad A_3 > 0, \quad A_1 A_2 - A_3 > 0 \quad (\text{B5})$$

Using the approximation for $\sin\psi_s$ from (A22), the first condition of (B5) becomes

$$[(Q_A + Q_B)(1 - q^2) + 2q^2] \sqrt{(1 - q^2)} + 8\eta\tau_N q \sin\phi_s > 0 \quad (\text{B6})$$

For *non-zero detuning*, the value of ϕ_s from the solution of (B6) can be used to find the corresponding condition on detuning from (A20), again with (A22), as

$$\Delta\Omega \cong \frac{2\eta}{\sqrt{1 - q^2}} (\alpha_H \sin\phi_s + q \cos\phi_s) \quad (\text{B7})$$

For *zero detuning*, $\tan\phi_s \cong -q/\alpha_H$ and the *tilted in-phase* solution has positive $\cos\phi_s$ so $\sin\phi_s \cong -q/\sqrt{\alpha_H^2 + q^2}$, and hence (B6) gives

$$[(Q_A + Q_B)(1 - q^2) + 2q^2] \sqrt{(1 - q^2)(\alpha_H^2 + q^2)} - 8\eta\tau_N q^2 > 0 \quad (\text{B8})$$

For *zero detuning*, the *tilted antiphase* solution gives the result

$$[(Q_A + Q_B)(1 - q^2) + 2q^2] \sqrt{(1 - q^2)(\alpha_H^2 + q^2)} + 8\eta\tau_N q^2 > 0 \quad (\text{B9})$$

Using the approximation for $\sin\psi_s$ from (A23), the second condition of (B5) becomes

$$2\eta\tau_p \left\{ [\Pi(1 - q^2) + 2] (q^2 \sin^2\phi_s + \cos^2\phi_s) + 2q\Pi \sin\phi_s (1 - q^2) (\alpha_H \cos\phi_s - q \sin\phi_s) \right\} > \Pi(1 - q^2)^{3/2} (\alpha_H \cos\phi_s - q \sin\phi_s) \quad (\text{B10})$$

For *non-zero detuning*, the LHS of (B10) is normally much less than the RHS since $\eta\tau_p \ll 1$. Hence (B10) implies that the RHS is less than zero, i.e., the SN bifurcation is given by $\alpha_H \cos\phi_s < q \sin\phi_s$. Substituting this into (B7) yields the result for the SN bifurcation

$$|\Delta\Omega| < 2\eta \sqrt{\frac{\alpha_H^2 + q^2}{1 - q^2}} \quad (\text{B11})$$

For equal pumping (B11) reduces to (30) of [16] (with $\eta_i = 0$).

For zero detuning, the tilted in-phase solution for the second condition of (B5) becomes

$$\begin{aligned} & \{(Q_A + Q_B - 2)(1 - q^2) [\alpha_H^2 (1 - 2q^2) - q^4] \\ & + 2(\alpha_H^2 + q^4)\} 2\eta\tau_p \\ & - (Q_A + Q_B - 2)(1 - q^2)^{3/2} (\alpha_H^2 + q^2)^{3/2} > 0 \quad (\text{B12}) \end{aligned}$$

For equal pumping (B12) reduces to $\eta > \alpha_H(Q - 1)/(2\tau_p Q)$, a result first derived by Winful and Wang in 1988 [26].

For zero detuning, the tilted antiphase solution for the second condition of (B5) becomes

$$\begin{aligned} & \{(Q_A + Q_B - 2)(1 - q^2) [\alpha_H^2 (1 - 2q^2) - q^4] \\ & + 2(\alpha_H^2 + q^4)\} 2\eta\tau_p \\ & + (Q_A + Q_B - 2)(1 - q^2)^{3/2} (\alpha_H^2 + q^2)^{3/2} > 0 \quad (\text{B13}) \end{aligned}$$

The third condition of (B5) can be simplified by only retaining the terms in $1/\tau_p$. Using the approximation for $\sin\psi_s$ from (A22), this gives

$$\begin{aligned} & [(Q_A + Q_B)(1 - q^2) + 2q^2] \sqrt{1 - q^2} \\ & + 4\eta\tau_N (\alpha_H \cos\phi_s + q \sin\phi_s) > 0 \quad (\text{B14}) \end{aligned}$$

For the case of equal pumping, (B14) reduces to equation (B27) of [16] (with $\eta_i = 0$).

Equations (B6), (B11) and (B14) correspond, respectively, to equations (13) – (15) of the main text.

For zero detuning, in the tilted in-phase case the result is

$$\begin{aligned} & [(Q_A + Q_B)(1 - q^2) + 2q^2] \sqrt{(1 - q^2)(\alpha_H^2 + q^2)} \\ & + 4\eta\tau_N (\alpha_H^2 - q^2) > 0 \quad (\text{B15}) \end{aligned}$$

For zero detuning, in the tilted antiphase case the result is

$$\begin{aligned} & [(Q_A + Q_B)(1 - q^2) + 2q^2] \sqrt{(1 - q^2)(\alpha_H^2 + q^2)} \\ & - 4\eta\tau_N (\alpha_H^2 - q^2) > 0 \quad (\text{B16}) \end{aligned}$$

For equal pumping, (B16) reduces to $\eta < Q/(2\alpha_H\tau_N)$, also first derived in [26]. Note that these and other authors use the notation $P = (Q - 1)/2$ for the normalised excess currents.

ACKNOWLEDGMENT

The authors are indebted to Dr. A. Hurtado (University of Strathclyde) for helpful discussions. Mike Adams thanks Dr. M. J. Holmes for checking some details of the calculations.

REFERENCES

- [1] Z. Gao, S. T. M. Fryslie, B. J. Thompson, P. Scott Carney, and K. D. Choquette, "Parity-time symmetry in coherently coupled vertical cavity laser arrays," *Optica*, vol. 4, no. 3, pp. 323–329, Mar. 2017.
- [2] Y. Kominis, V. Kovanis, and T. Bountis, "Controllable asymmetric phase-locked states of the fundamental active photonic dimer," *Phys. Rev. A*, vol. 96, no. 4, Oct. 2017, Art. no. 043836.
- [3] G. Pan *et al.*, "Analysis of optical coupling behavior in two-dimensional implant-defined coherently coupled vertical-cavity surface-emitting laser arrays," *Photon. Res.*, vol. 6, no. 11, pp. 1048–1055 Nov. 2018.
- [4] H. Dave, S. T. M. Fryslie, Z. Gao, B. J. Thompson, and K. D. Choquette, "Static and dynamic properties of coherently-coupled photonic crystal vertical cavity surface emitting laser arrays," *IEEE J. Sel. Topics Quantum Electron.*, vol. 25, no. 6, Nov./Dec. 2019, Art. no. 1700208.
- [5] M. T. Johnson, D. F. Siriani, M. P. Tan, and K. D. Choquette, "Beam steering via resonance detuning in coherently coupled vertical cavity laser arrays," *Appl. Phys. Lett.*, vol. 103, no. 20, Nov. 2013, Art. no. 201115.
- [6] M. T. Johnson, D. F. Siriani, M. P. Tan, and K. D. Choquette, "High speed beam steering with phased vertical cavity laser arrays," *IEEE J. Sel. Topics Quantum Electron.*, vol. 19, no. 4, Jul./Aug. 2013, Art. no. 1701006.
- [7] S. T. M. Fryslie, M. P. T. Siriani, D. F. Siriani, M. T. Johnson, and K. D. Choquette, "37-GHz modulation via resonance tuning in single-mode coherent vertical-cavity laser arrays," *IEEE Photon. Technol. Lett.*, vol. 27, no. 4, pp. 415–418, Feb. 2015.
- [8] S. T. M. Fryslie *et al.*, "Modulation of coherently coupled phased photonic crystal vertical cavity laser arrays," *IEEE J. Sel. Topics Quantum Electron.*, vol. 23, no. 6, Nov./Dec. 2017, Art. no. 1700409.
- [9] H. Dave *et al.*, "Digital modulation of coherently-coupled 2×1 vertical-cavity surface-emitting laser arrays," *IEEE Photon. Technol. Lett.*, vol. 31, no. 2, pp. 173–176, Jan. 2019.
- [10] Y. Kominis, K. D. Choquette, A. Bountis, and V. Kovanis, "Antiresonances and ultrafast resonances in a twin photonic oscillator," *IEEE Photon. J.*, vol. 11, no. 1, Feb. 2019, Art. no. 1500209.
- [11] Y. Kominis, A. Bountis, and V. Kovanis, "Radically tunable ultrafast photonic oscillators via differential pumping," *J. Appl. Phys.*, vol. 127, no. 8, Feb. 2020, Art. no. 083103.
- [12] Z. Gao, M. T. Johnson, and K. D. Choquette, "Rate equation analysis and non-Hermiticity in coupled semiconductor laser arrays," *J. Appl. Phys.*, vol. 123, no. 17, May 2018, Art. no. 173102.
- [13] Z. Gao, B. J. Thompson, H. Dave, S. T. M. Fryslie, and K. D. Choquette, "Nonhermiticity and exceptional points in coherently coupled vertical cavity laser diode arrays," *Appl. Phys. Lett.*, vol. 114, no. 6, Feb. 2019, Art. no. 061103.
- [14] Y. Kominis, V. Kovanis, and T. Bountis, "Spectral signatures of exceptional points and bifurcations in the fundamental active photonic dimer," *Phys. Rev. A*, vol. 6, no. 5, Nov. 2017, Art. no. 053837.
- [15] Y. Kominis, K. D. Choquette, A. Bountis, and V. Kovanis, "Exceptional points in two dissimilar coupled diode lasers," *Appl. Phys. Lett.*, vol. 113, no. 8, Aug. 2018, Art. no. 081103.
- [16] M. J. Adams, N. Li, B. R. Cemlyn, H. Susanto, and I. D. Henning, "Effects of detuning, gain-guiding, and index antiguiding on the dynamics of two laterally coupled semiconductor lasers," *Phys. Rev. A*, vol. 95, no. 5, May 2017, Art. no. 053869.
- [17] H. Dave, "Enhanced digital modulation of coherently coupled vertical cavity laser arrays: Theory and application," Ph.D. dissertation, Dept. Elect. Eng., Univ. Illinois at Urbana-Champaign, Urbana, IL, USA, 2020.
- [18] A. M. Mancho, S. Wiggins, J. Curbelo, and C. Mendoza, "Lagrangian descriptors: A method for revealing phase space structures of general time dependent dynamical systems," *Commun. Nonlinear Sci. Numer. Simulat.*, vol. 18, no. 12, pp. 3530–3557, Dec. 2013.
- [19] R. Al-Seyab, K. Schires, A. Hurtado, I. D. Henning, and M. J. Adams, "Dynamics of VCSELs subject to optical injection of arbitrary polarization," *IEEE J. Sel. Topics Quantum Electron.*, vol. 19, no. 4, Jul./Aug. 2013, Art. no. 1700512.
- [20] T. Erneux, J. Danckaert, K. Panajotov, and I. Veretenicoff, "Two-variable reduction of the san Miguel–Feng–Moloney model for vertical-cavity surface-emitting lasers," *Phys. Rev. A*, vol. 59, no. 6, pp. 4660–4667, Jun. 1999.
- [21] G. Van der Sande, J. Danckaert, I. Veretenicoff, and T. Erneux, "Rate equations for vertical-cavity surface-emitting lasers," *Phys. Rev. A*, vol. 67, no. 1, Jan. 2003, Art. no. 013809.
- [22] G. Van der Sande, L. Gelens, P. Tassin, A. Scirè, and J. Danckaert, "Two-dimensional phase-space analysis and bifurcation study of the dynamical behaviour of a semiconductor ring laser," *J. Phys. B: At. Mol. Opt. Phys.*, vol. 41, no. 9, May 2008, Art. no. 095402.
- [23] M. Adams, N. Li, B. Cemlyn, H. Susanto, and I. Henning, "Algebraic expressions for the polarisation response of spin-VCSELs," *Semicond. Sci. Technol.*, vol. 33, no. 6, Jun. 2018, Art. no. 064002.
- [24] T. Erneux, and D. Lenstra, "Synchronization of mutually delay-coupled quantum cascade lasers with distinct pump strengths," *Photonics*, vol. 6, no. 4, Dec. 2019, Art. no. 125.
- [25] H. Dave, Z. Gao, and K. Choquette, "Complex coupling coefficient in laterally coupled microcavity laser diode arrays," *Appl. Phys. Lett.*, vol. 117, no. 4, Jul. 2020, Art. no. 041106.
- [26] H. G. Winful, and S. S. Wang, "Stability of phase locking in coupled semiconductor laser arrays," *Appl. Phys. Lett.*, vol. 53, no. 20 pp. 1894–1896, Nov. 1988.
- [27] M. J. Adams, D. Jevtics, M. J. Strain, I. D. Henning, and A. Hurtado, "High-frequency dynamics of evanescently-coupled nanowire lasers," *Sci. Rep.*, vol. 9, Apr. 2019, Art. no. 6126.

Mike Adams received the Ph.D. degree in laser theory from the University of Wales, Cardiff, U.K., in 1970. Since 1996, he has been a Professor with the University of Essex, Colchester, U.K. He is involved in optoelectronics research and development with 15 years of experience in industry (Plessey, BT) and 35 years in academia with the University of Cardiff, University of Southampton, Southampton, U.K., and University of Essex. He has authored or coauthored widely in the optoelectronics field over many years, including a standard text on optical waveguide theory and two books on semiconductor lasers and optical fibres for use in telecommunications.

Rihab Al Seyab received the B.Sc. and M.Sc. degrees in electrical engineering from the University of Basrah, Basra, Iraq, in 1997, the Ph.D. degree in model predictive control from the University of Cranfield, Cranfield, U.K., in 2006, and the Ph.D. degree from the Dynamics of Spin-VCSELs (EPSRC Scholarship), University of Essex, Colchester, U.K., in 2013. She was a Senior Research Fellow with the University of Essex, in 2014, a Senior Design Engineer with CIP Technologies, Huawei, Ipswich, U.K., during 2015–2016, a Principle lecturer and the Deputy Head of the System Engineering Department, MTC, Oman, during 2016–2019. She is currently a Senior Lecturer and an Academic Course Leader of the M.Sc. Engineering programs with the School of Computing and Engineering, University of Gloucestershire, Cheltenham, U.K. She is also a Visiting Fellow with Prof. Mike Adams and Prof. Ian Henning, University of Essex.

Ian Henning received the B.Sc. degree (Hons.) in applied physics and the Ph.D. degree from the University of Wales, Cardiff, U.K. He was with British Telecom Research Laboratories, Martlesham Heath, in the Devices Division specializing mainly in the theory and measurement of semiconductor lasers. In 2002, he was a Professor with the Department of Electrical Systems Engineering, University of Essex, Colchester, U.K.

Hadi Susanto received the B.Sc. degree (Hons.) in mathematics from Institut Teknologi Bandung, Bandung, Indonesia, in 2001 and the Ph.D. degree from the University of Twente, Enschede, The Netherlands, in 2006. He then immediately joined the University of Massachusetts Amherst, Amherst, MA, USA, as a Visiting Assistant Professor. In 2008, he moved to the University of Nottingham, Nottingham, U.K., as a Lecturer of applied mathematics. In 2014, he joined the University of Essex, Colchester, U.K., as a Senior Lecturer and then a Professor of applied mathematics (currently on-leave). He is currently a Professor with Khalifa University, Abu Dhabi, UAE. He has worked mainly in the areas of nonlinear waves, differential equations, and mathematical modeling.

Martin Vaughan received the Ph.D. degree from the University of Essex, Colchester, U.K., in 2007. He was a Postdoctoral with the University of Essex. In 2009, he moved to Tyndall National Institute, Cork, Ireland, and later held a lectureship with the University College Cork. He returned to the U.K. in 2017, where he joined the University of Bristol, Bristol, U.K. In 2018, he moved back to the University of Essex.